Numerical Simulation of Droplet Combustion using Volume-of-Fluid Method

TADASHI WATANABE
Research Institute of Nuclear Engineering
University of Fukui
Kanawa-cho 1-3-33, Tsuruga-shi, Fukui-ken, 914-0055
JAPAN
twata@u-fukui.ac.jp http://www.rine.u-fukui.ac.jp/watanabe/

Abstract: - The droplet combustion is simulated numerically. The Navier-Stokes equations and the energy conservation equations together with the combustion model equations are solved in the computational fluid dynamics framework using the volume-of-fluid method. The characteristics of temperature increase due to combustion are simulated well, and the effect of ambient flow is made clear. It is shown that the droplet shape is varying and the high temperature region spreads widely in the ambient flow. The internal vortex flow is found to be driven by the surface tension force. The present numerical model is effective for analyses of complicated reacting flows.

Key-Words: Simulation, Droplet, Combustion, CFD, VOF, Vortex

1 Introduction

The leakage of liquid sodium is one of the important phenomena during the core disruptive accident of sodium cooled fast breeder nuclear reactors. Sodium is highly reactive, and its leakage or discharge into air results in explosive fire. The spray type discharge is serious since the spray is composed of a large number of small droplets [1], and the reaction area between sodium and air becomes large. The droplet combustion is the fundamental process of sodium fire during the accident, and thus the understanding of its detail is essential for safety evaluation of nuclear reactors.

Experiments of a falling sodium droplet in air have been performed [2-4]. Burning rates and falling velocities were obtained by changing the droplet size and falling distance. The experimental data were analysed using the simple model, in which the droplet was represented by a solid particle, and the reasonable agreement with the experimental data was shown. The solid particle model is also used in some computer codes for sodium combustion [5,6]. The internal flow field and the shape of burning droplet were not discussed in these studies. The combustion of a suspended sodium droplet has been observed experimentally [7-10], and the temperature variation in the burning droplet was obtained. The effect of ambient air flow on the droplet temperature was shown by changing the flow velocity. The flow fields in and around the droplet and the droplet shape were, however, not discussed.

Numerical simulations have been performed for the falling sodium droplet [11] and for the sodium droplet in the air flow [12]. The chemical reaction around the droplet was discussed, but the internal flow field was not calculated. The spray fire was numerically studied [13] using the chemical kinetics model. The droplet was, however, treated as a solid sphere as in the previous analyses and simulations, and the characteristics of the liquid droplet was not considered so far.

In this study, a computational fluid dynamics (CFD) model for the droplet combustion is proposed based on the volume-of-fluid (VOF) method. The droplet is treated as a liquid droplet, and the internal flow and the shape variation are calculated. The combustion of suspended sodium droplet [9] is simulated as an example of droplet combustion. The increase in droplet temperature is compared with the experimental result, and the flow fields in and around the droplet are discussed.

2 Numerical Model

2.1 Flow field

The flow field including the burning droplet is simulated using the CFD software ANSYS Fluent [14]. The Navier-Stokes equations together with the mass and energy conservation equations are solved by the finite volume method. The VOF model, in which the transport equation of volume fraction is solved, is used to simulate the motion of droplet surface. The volume fraction of liquid is unity in the

droplet region and zero in the ambient gas region. The fluid properties such as the viscosity and the density are interpolated across the droplet surface according to the volume fraction.

The first order implicit method is used for time integration and the third order monotone upstream-centered scheme for conservation laws (MUSCL) is used for spatial discretization. The pressure-implicit with splitting of operators (PISO) method is used for calculations of pressure and velocity. These numerical methods are selected from the viewpoint of numerical accuracy and stability by pre-test calculations.

2.2 Combustion reaction

The outline of combustion reaction, which is the energy source for the flow field, is described in the following. The surface oxidation reaction occurs as the pre-ignition stage when the sodium droplet with relatively low temperature is released into the atmospheric air. The droplet temperature increases due to the reaction heat on the droplet surface until it reaches the ignition condition. After ignition, the combustion in vapor phase occurs due to the evaporation of sodium from the droplet surface since the droplet temperature is sufficiently high. This is the post-ignition stage. The ignition temperature in the atmosphere is reported to be 850 K based on the experimental observation [9].

Two chemical reactions occur mainly during the sodium combustion:

$$4Na + O_2 \rightarrow 2Na_2O \quad , \tag{1}$$

$$2Na + O_2 \rightarrow Na_2O_2 \quad . \tag{2}$$

The sodium monoxide in Eq. (1) is the main product when the droplet temperature is below 800 K [15]. It is reported [4] for the temperature above 850 K that the reaction is composed of 60 % of sodium monoxide reaction given by Eq. (1) and 40 % of sodium peroxide reaction given by Eq. (2). Thus in this study, Eq. (1) is considered for the pre-ignition stage below the droplet temperature of 850 K and Eqs. (1) and (2) are considered for the post-ignition stage above 850 K.

The surface reaction rate under relatively low temperature conditions before ignition is modeled using the chemical kinetics model [15]:

$$r = \upsilon W_{Na} (\rho_g Y_O / W_O)^n B_s \exp[-E/(RT)] \quad , \tag{3}$$

where r is the reaction rate, ν the stoichiometric coefficient, ρ the density, W the molecular weight, Y the mole fraction, n the reaction order, B_s the frequency factor of the surface reaction, E the activation energy, R the universal gas constant, T the temperature, and the subscripts Na, g and O denote sodium, ambient gas and oxygen, respectively. The frequency factor is 320 m/s and the constant E/R is 6350 K according to the experiment.

The vapor phase combustion after ignition is modeled using the mass transfer rate of oxygen. The vapor reaction rate under high temperature condition is given by [13]

$$r = 4M_O \quad , \tag{4}$$

where M_o indicates the mass transfer rate of oxygen from the ambient gas to the reaction zone. This equation corresponds to the reaction given by Eq. (1), and the reaction rate of sodium is four times larger than the reaction rate of oxygen. Equation (1) is considered alone in the original model, and the coefficient in Eq. (4) is always four [13]. In this study, however, the reactions given by Eqs. (1) and (2) are considered for the post-ignition stage according to the experiment [4], and the coefficient is four for Eq. (1) and two for Eq. (2). The mass transfer rate is calculated using the mole fraction of oxygen.

$$M_O = K_c (\rho_g / W_O)(Y_O - Y_{Of}) \quad , \tag{5}$$

where K_c is the mass transfer coefficient and Y_{Of} is the mole fraction of oxygen at the reaction zone, which is calculated by taking into account the saturation vapor pressure of sodium. The mass transfer coefficient is evaluated using the following equation based on the flow field.

$$K_c = (D/d)(2.0 + 0.6\,\mathrm{Re}^{0.5} Sc^{0.33}) \tag{6}$$

where D is the molecular diffusivity and d is the droplet diameter, Re and Sc are, respectively, the Reynolds number and the Schmidt number defined by the following equations.

$$\mathrm{Re} = (\rho_g u d / \mu_g) \quad , \tag{7}$$

$$Sc = [\mu_g / (\rho_g D)] \quad , \tag{8}$$

where μ_g is the viscosity of the ambient gas.

2.3 Energy source term

The above described reaction model is implemented into the code using the user defined function of Fluent as a source term in the energy conservation equations. The energy source term is calculated by using the reaction rate.

$$S = qr\Delta s \quad , \tag{9}$$

where S is the source term in the energy equations, q the reaction heat, and Δs the reaction area. The reaction area corresponds to the interfacial area between droplet and air in the calculation cell, and is obtained as a function of volume fraction [16,17].

$$\Delta s = \pi l^2 \alpha (1-\alpha) \quad , \tag{10}$$

where l is the cell size and α is the volume fraction of gas or the void fraction. The interfacial area is zero in the pure droplet region with the gas volume fraction of zero and in the pure gas region with the gas volume fraction of unity. The cell size in Eq. (10) is given by

$$V = (\pi / 6) l^3 \quad , \tag{11}$$

where V is the volume of the calculation cell. The evaluation method for the interfacial area using Eqs. (10) and (11) are very effective especially in the framework of CFD code, since the interfacial area is not used in the governing equations for the fluid motion, but the volume fraction is used in the VOF model.

2.4 Numerical condition

A single sodium droplet suspended in the flowing air is simulated in this study. The simulation conditions are almost the same as those used in the experiment [9]. The size of the simulation region is 12.0 mm x 12.0 mm. The sodium droplet, which is suspended at the lower end of a thin vertical support tube, is located at the center of the simulation region. The direction of the flowing air is upward from the bottom inlet. The droplet diameter is 4.0 mm and the initial temperature is 673 K. The inlet air temperature is 303 K and the flow velocity is ranging from 0.2 m/s to 0.6 m/s. The outflow and slip boundary conditions are, respectively, applied at the top and side boundaries. The simulation region is divided into 60 x 60 equal-size calculation cells.

The volume fraction is gradually varied in between the pure droplet and air regions as shown in the following section. The location with the volume fraction of 0.5 is usually regarded as the interface, and it is assumed that the surface reaction occurs slightly in the droplet side with the liquid volume fraction from 0.5 to 0.8, while the vapor reaction occurs in the air side with the gas volume fraction from 0.7 to 0.8.

3 Results and Discussion

3.1 Temperature increase

The time history of the droplet temperature obtained at the center location is shown in Fig. 1, along with the experimental data obtained by the thermocouple inserted into the droplet through the side surface. Three cases with different air velocity are shown. The droplet temperature increases from the initial temperature due to the pre-ignition surface reaction. The temperature shows exponential increase during the pre-ignition stage up to the ignition temperature of 850 K at about 0.75 s, and the increase rate becomes small after ignition. The agreement between the numerical simulation and the experiment is good up to 1.5 s.

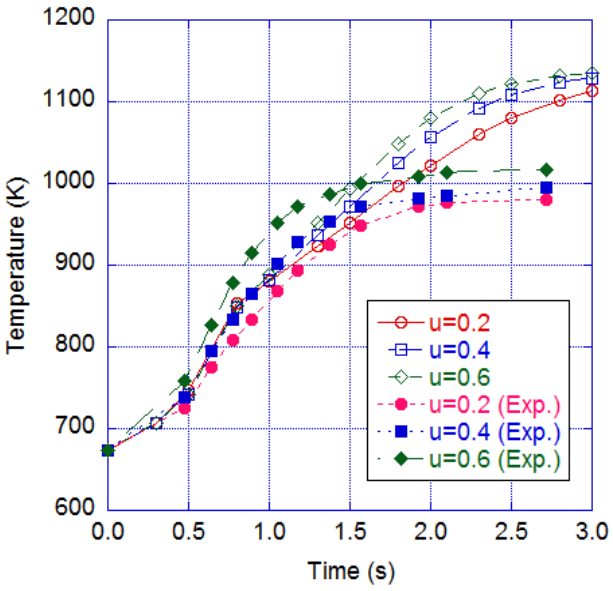

Fig. 1: Time history of droplet temperature.

The droplet temperature continues to increase in the simulation, though the increase rate becomes small, while the experimental temperature seems to reach the maximum value of about 1000 K. The boiling temperature of sodium is about 1156 K, and it was reported in the experiment [9] that the low maximum temperature in the observation was probably due to the heat loss through the support tube and the thermocouple. The low maximum temperature is also reported in a similar experiment using the suspended sodium droplet with a support

tube and a thermocouple [18]. The heat conduction of the support tube is not modeled in this study and the thermocouple is not included. The evaluation of these structural effects on the maximum droplet temperature would be desirable for detailed comparison.

The effect of air flow is shown clearly in Fig. 1. The increase rate of temperature is larger for the cases with larger flow velocity. The effect of air flow is included in Eq. (6) in terms of *Re*, and the reaction heat due to oxygen supply is found to be larger than the heat transfer due to cooling. The characteristics of temperature increase are shown to be simulated well by the present model.

3.2 Droplet shape and temperature distribution

The distributions of volume fraction and temperature are, respectively, shown in the upper and lower parts of Fig. 2. These examples are obtained at 1.0 s, 2.0 s and 3.0 s of the case with the inlet flow velocity of 0.6 m/s. In the upper part, the volume fraction of liquid sodium is indicated by red, while that of air by blue. The temperature range is from 300 K indicated by blue to 1135 K by red in the lower part.

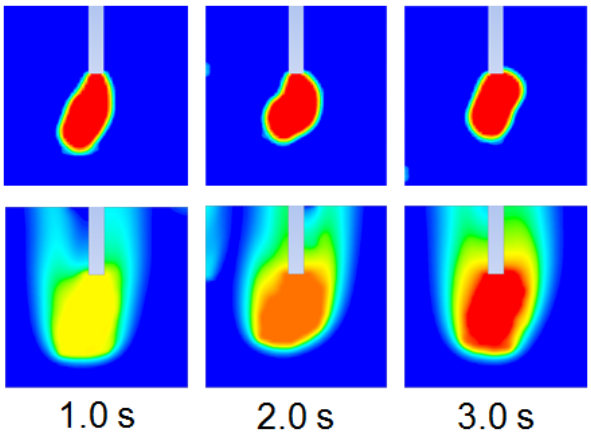

Fig. 2: Distributions of volume fraction (upper) and droplet temperature (lower).

It is shown that the droplet shape is always varying, and the high temperature region in air corresponds to the droplet shape. It is seen that the high temperature region spreads widely from the droplet surface. The droplet temperature increases gradually with time, and the maximum temperature in the droplet is about 899 K at 1.0 s, 1084 K at 2.0 s and 1135 K at 3.0 s. The droplet temperature seems to be uniform in Fig. 2, but the maximum temperature is obtained near the bottom of the droplet, which is the front side to the air flow. The maximum temperature is, thus, slightly different from the center temperature shown in Fig. 1.

The distributions of liquid volume fraction along the vertical center axis through the droplet are shown in Fig. 3. The vertical location of 0.0 m corresponds to the air inlet. The distribution at 0.0 s is for the initial condition, and the liquid volume fraction is zero and unity, respectively, below and above the bottom surface of the droplet at 0.004 m. The droplet diameter is 0.004 m and the initial droplet center is at 0.006 m in Fig. 3. It is seen that the bottom of the droplet moves downward due to gravity and is varying with time as shown in Fig. 2.

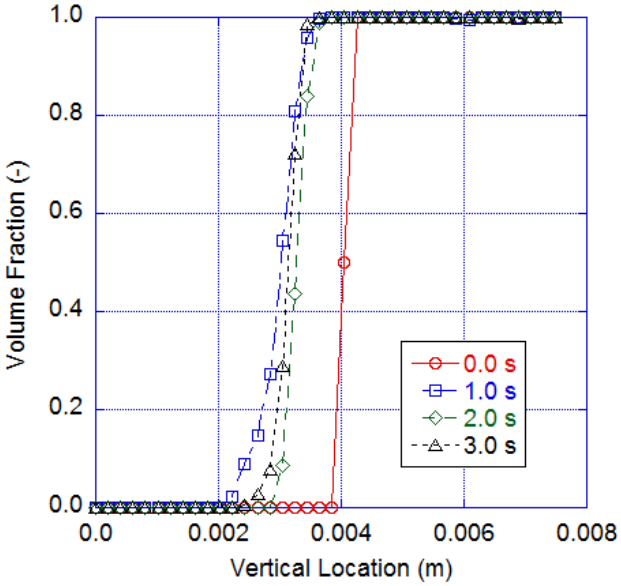

Fig. 3: Vertical distribution of liquid volume fraction.

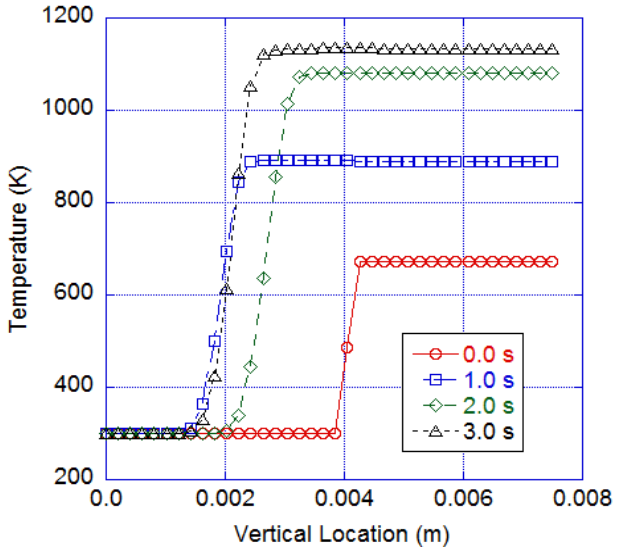

Fig. 4: Vertical distribution of droplet temperature.

The temperature distributions along the vertical center axis are shown in Fig. 4. The distribution at 0.0 s is for the initial condition and the temperature in the droplet above the bottom surface is higher than the air temperature. The droplet temperature increases with time due to the reaction heat as shown in Figs. 1 and 2. The temperature in the droplet seems to be uniform as shown in Fig. 2, but is slightly higher near the bottom surface. It is found in Figs. 3 and 4 that the temperature starts to increase in the air region below the bottom surface of the droplet. In other words, the high temperature region spreads widely upstream in the air. This corresponds to the widespread temperature distribution shown in Fig. 2.

3.3 Effect of reaction

In this study, the droplet combustion is simulated, and the temperatures in the droplet and the ambient air increase due to the reaction heat. The effects of reaction on the droplet temperature and the air flow are shown here. The time history of the droplet temperature without reaction is shown in Fig. 5. The simulation conditions other than the reaction are the same as the cases shown in Fig. 1.

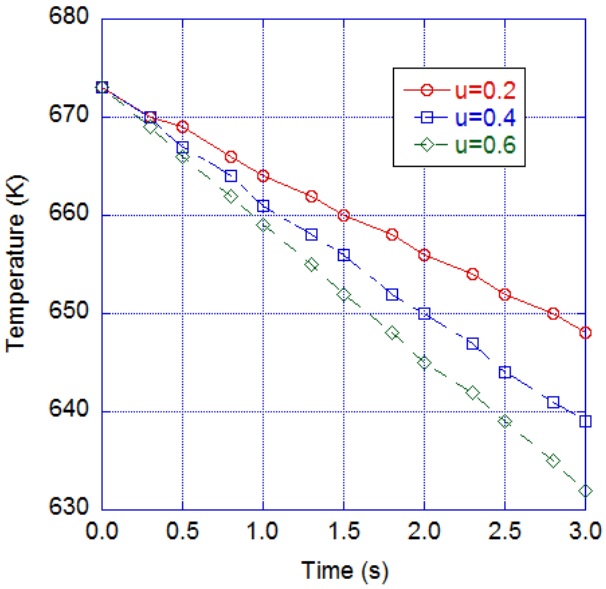

Fig. 5: Time history of droplet temperature without reaction.

It is shown clearly that the droplet temperature simply decreases due to cooling. The decrease rate is larger for the cases with larger air flow velocity. The heat transfer due to cooling is governed by the air flow. The temperature and velocity of ambient air flow are constant, and the droplet temperature decreases linearly as seen in Fig. 5. It is noted for the case without reaction that the droplet shape is varying too as was the case with reaction.

The effect of reaction on velocity distribution is shown in Fig. 6. The droplet shape is varying with time as shown in Fig. 2, and thus the average velocity is compared here. The average vertical velocity is calculated along the horizontal line through the initial droplet center at the vertical location of 0.006 m. The average velocity is obtained over the time period from 1.0 s to 3.0 s. The results with no reaction are indicated by NR in Fig. 6, and positive and negative vertical velocities, respectively, indicate the upward and downward flows.

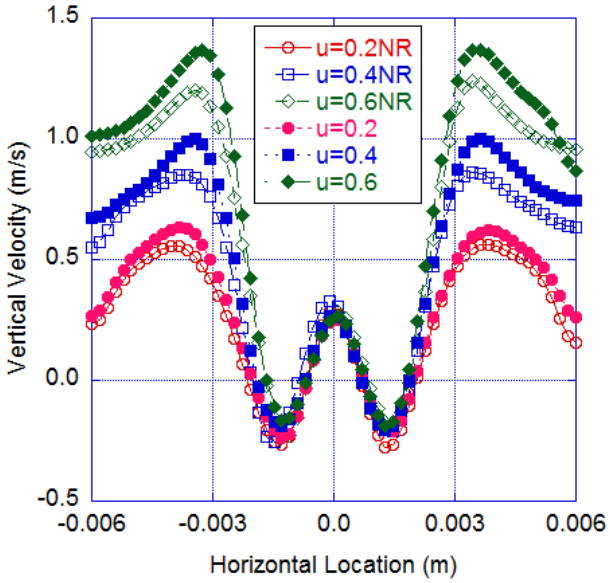

Fig. 6: Effect of reaction on velocity distribution.

It is shown in Fig. 6 that the air flow outside the droplet is upward and the average velocity is larger for the cases with reaction. The air flow is thus found to be accelerated by the reaction heat. In the droplet region from about -0.002 m to 0.002 m, however, the downward flows appear near the surface and the upward flow is seen in the center. This velocity distribution indicates vortices in the droplet. It is noted that the average internal flow is almost the same for all cases shown in Fig. 6 and not affected by the outside air flow and reaction.

3.4 Internal flow field

The internal flow fields at 1.0 s, 2.0 s and 3.0 s of the case with the inlet velocity of 0.6 m/s are shown in Fig. 7, where the pressure distribution and the velocity vector are, respectively, shown in the upper and lower parts. The pressure distribution indicates the relative pressure normalized between the

maximum and the minimum values in each time step. The pressure distribution in Fig. 7 is seen to be varying with time according to the shape variation shown in Fig. 2. It is shown that the pressure near the convex surface is always higher and that near the concave surface is lower. It is thus found that the pressure distribution corresponds to the surface tension force.

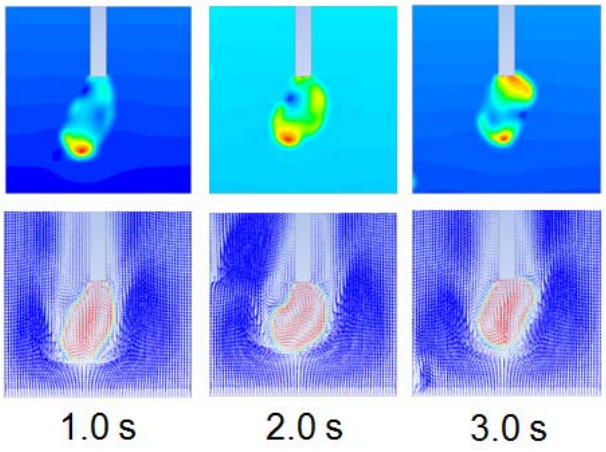

Fig. 7: Pressure distribution (upper) and velocity vector (lower).

The velocity vector in the lower part of Fig. 7 shows clearly the vortex flow in the droplet. The upward and downward flows appear, respectively, in the center and near the side surface. The upward flow seems to start from the high pressure region near the bottom surface shown in the pressure distribution. It is indicated that the internal vortex flow is driven by the surface tension force, since the bottom surface is always convex.

In order to see the effect of surface tension force, the surface tension of droplet is changed in Fig. 8 as a parameter study. The average velocity in the vertical direction is shown for three cases with different surface tension: a factor of 1.0, 1.5, and 2.5 for the original surface tension. It is seen that the upward flow in the outside air is not much affected by the surface tension. The internal vortex flow is qualitatively the same for three cases, but the magnitude is different. The maximum flow velocity, in both the upward and downward flows, is larger for the cases with larger surface tension. The internal vortex flow is not affected by the outside air flow as shown in Fig. 6, and thus confirmed to be driven by the surface tension force.

It is noted that the internal vortex flow appears even for the case without reaction as shown in Fig. 6. The droplet temperature without reaction is uniform and decreases constantly as shown in Fig. 5. The temperature distribution is almost uniform too with reaction as shown in Fig. 4. The uniform temperature in the droplet with reaction is due to the internal vortex flow. The internal vortex flow with reaction is almost the same as that without reaction as shown in Fig. 6. This indicates that the internal vortex flow is driven by the surface tension but not by the Marangoni effect. The droplet shape is always slightly longer in the vertical direction, since the droplet is suspended. The internal pressure is always higher near the bottom surface as shown in Fig. 7 and the internal vortex flow appears in the suspended droplet. The suspended droplet was used to measure the temperature variation in the droplet [7-10], but it might not be suitable for studying the falling droplet.

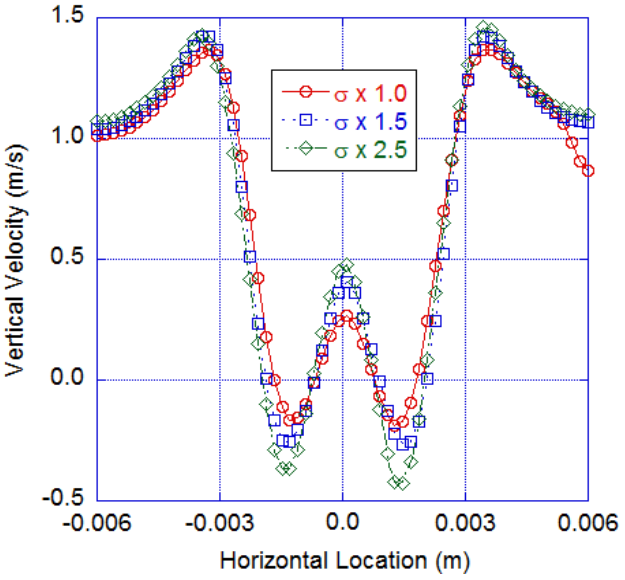

Fig. 8: Effect of surface tension on velocity distribution.

4 Conclusion

The combustion of sodium droplet has been simulated numerically in this study as an example of droplet combustion. The flow fields in and around the droplet were obtained by solving the Navier-Stokes equations and the energy conservation equations in the CFD framework. The motion of droplet surface was obtained by the VOF method. The reaction area was obtained using the volume fraction, and the reaction heat was implemented into the code as the source term in the energy conservation equations.

The characteristics of temperature increase due to combustion were simulated well by the present model, and the effect of ambient air flow was made clear. It was shown that the droplet shape was

varying with time and the high temperature region was spreading widely in the ambient air flow. The internal vortex flow was found to be driven by the surface tension force and not affected by the outside air flow. The shape variation and the internal flow field were not obtained by the previous numerical simulations in the literature, since the droplet was treated simply as a solid particle.

The present analytical model for droplet combustion is based on the CFD framework and the VOF model. The VOF model is widely used not only in the commercial codes but also in the open source code such as OpenFOAM, and it is easy to implement the present model into other CFD codes. The two-stage reaction model is used in this study, but it is also easy to use other reaction models with several-stage reactions or many species. The present model would thus be applicable for much complicated reacting flows such as a splay including many droplets.

References:

[1] K. Nagai, M. Hirabayashi, T. Onojima, et al., Sodium leakage and combustion tests. – Measurement and distribution of droplet size using various spray nozzles, 1999, JNC TN9400 99-030.

[2] S. Miyahara, K. Ara, Falling sodium droplet experiments, 1998, PNC TN9410 98-065.

[3] N. Doda, S. Ohno, S. Miyahara, Falling sodium droplet experiments (FD2), 2003, PNC TN9400 2003-011.

[4] N. Doda, S. Ohno, S. Miyahara, Falling sodium droplet experiments (FD3), 2005, PNC TN9400 2005-048.

[5] S. S. Tsai, The NACOM code for analysis of postulated sodium spray fires in LMFBRs, 1980, NUREG/CR-1405.

[6] S. Ohno, T. Matsuki, H. Ishikawa, et al., Sodium Combustion computer Code ASSCOPS Version 2.1 User's Manual, 2000, JNC TN9520 2000-001.

[7] K. Sato, K., Study on combustion behavior of sodium droplet, 2002, JNC TY9400 2003-008.

[8] K. Sato, An experimental study on suspended sodium droplet combustion, 2003, JNC TY9400 2004-003.

[9] K. Sato, An experimental study on suspended sodium droplet combustion (II), 2004, JNC TY9400 2004-022.

[10] K. Sato, An experimental study on suspended sodium droplet combustion (III), 2005, JNC TY9400 2005-005.

[11] Y. Okano, A. Yamaguchi, Numerical simulation of a free falling liquid sodium droplet combustion, *Annals of Nuclear Energy*, No. 30, 2003, pp. 1863–1878.

[12] P. Mangarjuna Rao, V. Raghavan, K. Velusamy, et al., Modeling of quasi-steady sodium droplet combustion in convective environment, *International Journal of Heat and Mass Transfer*, No. 55, 2012, pp. 734-743.

[13] S. M. Saravanan, P. M. Rao, B. K. Nashine, et al., NAFCON-SF: A sodium spray fire code for evaluating thermal consequences in SFR containment, *Annals of Nuclear Energy*, No. 90, 2016, pp. 389–409.

[14] *ANSYS, ANSYS FLUENT Theory Guide Release 14.0*, 2011.

[15] A. Makino, Ignition delay and limit of ignitability of a single sodium droplet: theory and experimental comparisons, *Combustion and Flame*, No. 134, 2003, pp. 149-152.

[16] T. Watanabe, H. Nakamura, CFD analysis of temperature stratification experiment in OECD/NEA ROSA project, *Proceedings of 13th International Topical Meeting on Nuclear Reactor Thermal Hydraulics*, 2009, N13p1158.

[17] J. Cai, T. Watanabe, Numerical simulation of thermal stratification in cold legs by using OpenFOAM, *Progress in Nuclear Science and Technology*, No. 2, 2011, pp. 107-113.

[18] M. Nishimura, H. Kamide, S. Otake, et al., Features of Dendritic Oxide during Sodium Combustion, *Journal of Nuclear Science and Technology*, No. 48(12), 2011, pp. 1420-1427.